Research Article

SURFACE and INTERFACE ANALYSIS

Received: 03 March 2008 Revised: 18 July 2008 Accepted: 28 July 2008 Published online in Wiley Interscience: 10 October 2008

(www.interscience.com) DOI 10.1002/sia.2936

Influence of the description of the target energy-loss function on the energy loss of swift projectiles

Cristian D. Denton,[a]* Isabel Abril,[a] Rafael Garcia-Molina,[b] Juan C. Moreno-Marín[c] and Santiago Heredia-Avalos[c]

The optical energy-loss function (ELF) of Au and Al, obtained from experiments, is extended to finite wavenumber *k* using three different widely used models, namely, with the Mermin type ELFs with generalized oscillator strengths (MELF-GOS) model, the extended Drude model and the Penn model. The resulting ELFs show important differences but the MELF-GOS model gives more realistic results when compared with the available experimental ELFs for finite *k*. These differences affect calculations of important parameters in projectile-solid interaction. The calculated stopping power and energy-loss straggling of Au and Al for H projectiles as well as the corresponding inelastic mean free path (IMFP) of electrons in Au and Al clearly show that the results depend on the model used for the ELF description. Comparison with experimental data gives support to the MELF-GOS model, especially in a material with a complex energy-loss spectrum such as Au.

Keywords: stopping power; energy loss; straggling; inverse mean free path; dielectric properties

Introduction

The interaction of charged projectiles with matter is affected by the inelastic excitations of the target electrons by the swift incident particle. In fact, these processes are the main source of slowing down for swift charged particles. A lot of applications and techniques need to know the energy loss of the projectile for quantitative purposes. Among them, it is worth mentioning the bombardment of tumors with ions for therapeutical purposes,[1] ion beam analysis techniques, like PIXE, RBS or ERDA,[2] or implantation of ions for doping of semiconductors, where the stopping power of the material is the key parameter. Other surface-spectroscopic techniques, such as Auger or photoelectron spectroscopies, use the mean free path for electronic inelastic excitations to obtain quantitative results from spectra.[3]

Knowing the energy-loss function (ELF) of a material and using the dielectric formalism,[4] it is possible to calculate the main momenta of the projectile energy-loss distribution. The ELF represents the probability that an excitation event with momentum transfer $\hbar k$ and energy transfer $\hbar\omega$ takes place in the target. Several experimental techniques[5] provide the ELF of a material at $k = 0$, which is called the optical limit. Nevertheless data for the ELF at $k \neq 0$ are scarce and there are several models to extend the optical ELF to finite k values,[6–10] but they yield somewhat different results, and hence, the inelastic energy loss calculated from the different approaches of the ELF could be different in principle.

Here we model the ELF of Au and Al using the Mermin type ELFs with generalized oscillator strengths (MELF-GOS) model,[9,11,12] the extended Drude model proposed by Ritchie and Howie[6,8] and the Penn model,[7,8] comparing the dependence of the ELF with k in the three models. We have chosen Au and Al because they represent extreme behavior for the optical ELF. The response of Al is similar to a free electron gas with a sharp single peak in the ELF, while Au has a complex and wide excitation spectrum. We also use these models to calculate the stopping power and the energy-loss straggling for protons, as well as the inelastic mean free path (IMFP) of electrons in Au and Al, in order to compare these quantities with available experimental data.

This article is structured as follows. In Section on Model we show how to describe the energy loss of projectiles within the dielectric formalism and we introduce three models to extend the optical ELF to $k \neq 0$. In Section on Results we obtain the ELF at finite k using the three models and study the influence on the stopping power and energy-loss straggling for protons in Au and Al, as well as the IMFP of electrons in Au and Al. The main conclusions are drawn at the end of this article.

Model

Energy loss of a projectile

When a projectile of charge q and velocity v penetrates a medium characterized by the dielectric function $\varepsilon(k, \omega)$, it produces electronic excitations in the medium, losing energy in the process. Here we deal with swift incident particles, so that the energy loss

* *Correspondence to: Cristian D. Denton, Departament de Física Aplicada, Universitat d'Alacant, Apartat 99, E-03080 Alacant, Spain. E-mail: denton@ua.es*

a *Departament de Física Aplicada, Universitat d'Alacant, Apartat 99, E-03080 Alacant, Spain*

b *Departamento de Fisica-ClOyN, Universidad de Murcia, Apartado 4021, E-30080 Murcia, Spain*

c *Departament de Física, Enginyeria de Sistemes i Teoria del Senyal, Universitat d'Alacant, Apartat 99, E-03080 Alacant, Spain*

due to elastic scattering with the target nuclei can be neglected. The target ELF, $\mathrm{Im}\left[-1/\varepsilon\,(k,\omega)\right]$, represents the probability that the projectile produces an electronic excitation with momentum transfer $\hbar k$ and energy transfer $\hbar\omega$.

Within the linear dielectric formalism,[4] the resulting energy-loss distribution of the projectiles per unit path length is characterized by the moments given by

$$\frac{\langle\Delta E^n\rangle}{\Delta x}=\frac{2}{\hbar\pi v^2}\int_0^{\omega\max}\mathrm{d}\omega(\hbar\omega)^n\int_{k_1(\omega)}^{k_2(\omega)}\frac{\mathrm{d}k}{k}F(k)^2\mathrm{Im}\left[\frac{-1}{\varepsilon(k,\omega)}\right], \tag{1}$$

where $F(k)$ is the Fourier transform of the projectile charge density. The limits of the integrals are related to energy conservation in the target-electron excitation process

$$k_{1,2}(\omega)=\frac{mv}{\hbar}\mp\sqrt{\frac{mv}{\hbar}-2\omega}\quad\text{and}\quad\omega_{\max}=\frac{mv^2}{2\hbar}, \tag{2}$$

with m being the electron mass.

When the mass of the projectile is large compared to the mass of the electron (for instance, for proton beams), the above limits can be written as $k_1=\omega/v$, $k_2\to\infty$ and $\omega_{\max}\to\infty$. The moment in Eqn (1) with $n=0$ corresponds to the inverse of the IMFP, which is the mean distance between consecutive inelastic electronic excitations. The stopping power S_p of the target is the first moment of the distribution, i.e. the mean energy lost by the projectile per unit path length. The second moment of the distribution is called the energy-loss straggling Ω^2 and represents the variance of the energy loss per unit path length. As can be observed from Eqn (1), a correct description of the ELF is necessary for a complete characterization of the energy-loss process, at least in the range of projectile velocities and charges where the linear dielectric theory is valid. Nowadays, there are a good number of materials whose optical ELF (at $k=0$) is available from experiments.[5] Unfortunately, experimental data of the ELF at $k\neq0$ is scarce.[13–17] Therefore, the dependence of the ELF with k has to be modelled in a proper manner. In the rest of this section, we describe three widely used models to account for the behavior of the ELF at finite k, and afterwards, we show how to apply the dielectric formalism for the calculation of the stopping power and the energy-loss straggling of a material being bombarded by protons; the inverse mean free path of electrons will also be calculated.

ELF description

MELF-GOS model

The MELF-GOS model uses different approaches for the contributions to the ELF of the target electronic excitations coming from outer- or inner-shell electrons. The former is obtained by fitting the experimental ELF in the optical limit ($k=0$) by a linear combination of Mermin-type ELF,[9,11,12]

$$\mathrm{Im}\left[\frac{-1}{\varepsilon(k=0,\omega)}\right]_\mathrm{outer}=\sum_i A_i\mathrm{Im}\left[\frac{-1}{\varepsilon_\mathrm{M}(\omega_i,\gamma_i;k=0,\omega)}\right]_{\omega\geq\omega_{\mathrm{th},i}}, \tag{3}$$

with ε_M being a Mermin-type dielectric function.[18] The fitting parameters ω_i, γ_i and A_i are related, respectively, to the position, width and relative weight of the peaks observed in the ELF spectrum; $\omega_{\mathrm{th},i}$ is a threshold energy. A Mermin ELF represents an improvement over the Lindhard ELF since it incorporates the broadening due to the lifetime of the excitations. The ELF fitted at $k=0$ is analytically extended to all values of k through the properties of the Mermin dielectric function,[19] so no dispersion schemes are necessary to incorporate the k dependence of the ELF.

The description of the contribution to the ELF coming from the inner-shell electrons is done in terms of the GOS for isolated atoms; this approach is suitable since inner-shell electrons have large binding energies and show negligible collective effects. The relation between the ELF and the GOS $\frac{\mathrm{d}f_{n\ell}}{\mathrm{d}\omega}$ of the $n\ell$ sub-shell is given by[20]

$$\mathrm{Im}\left[\frac{-1}{\varepsilon(k,\omega)}\right]_\mathrm{inner}=\frac{2\pi^2\mathcal{N}}{\omega}\sum_{n\ell}\frac{\mathrm{d}f_{n\ell}(k,\omega)}{\mathrm{d}\omega}, \tag{4}$$

where $\mathcal{N}$ is the atomic density of the target. The total ELF will be the sum of the contributions coming from the outer- and inner-shell electrons. The parameters of the ELF fitting in Eqn (3) are chosen in such a way that the ELF reproduces the main trends of the experimental optical ELF and satisfies the f-sum rule for every k,

$$Z_2=\frac{1}{2\pi^2\mathcal{N}}\int_0^\infty\mathrm{d}\omega\,\omega\mathrm{Im}\left[\frac{-1}{\varepsilon(k,\omega)}\right], \tag{5}$$

where Z_2 is the atomic number of the target. This fact imposes another restriction on the obtained ELF, because the contribution to the f-sum rule from the inner shells depends on k.[21] We have also checked that these fittings to the optical ELF satisfy the perfect screening sum rule within 7% for Au and 2% for Al. The MELF-GOS model has shown its accuracy and reliability in describing the k dependence of the ELF for Al, graphite and liquid water[19,22] as well as in calculating the stopping power and energy-loss straggling for several targets, both elemental or compounds, for light projectiles over a broad range of incident energies.[11,23–27] In Ref. [28], De la Cruz and Yubero used a variant of this model to study the IMFP of electrons in solids. The main difference between the MELF-GOS model presented here and that used by De la Cruz and Yubero is in the treatment of the inner-shells. Previously,[9] the fitting of the contribution to the ELF coming from the inner-shells was done with truncated Mermin ELFs, choosing a quadratic dispersion in the threshold in order to satisfy the f-sum rule; now we use GOS, which are much more *ad hoc* to describe the response of an inner-shells.

Extended Drude model

Ritchie and Howie[6] proposed an extension to $k\neq0$ of the Drude model in which the fitting of the optical ELF corresponding to the outer-shell electrons is obtained through Drude-type ELFs

$$\mathrm{Im}\left[\frac{-1}{\varepsilon(k=0,\omega)}\right]_\mathrm{outer}=\sum_i B_i\mathrm{Im}\left[\frac{-1}{\varepsilon_\mathrm{D}(\omega_i,\gamma_i;k=0,\omega)}\right]_{\omega\geq\omega_{\mathrm{th},i}}, \tag{6}$$

and each Drude-type ELF takes the form

$$\mathrm{Im}\left[\frac{-1}{\varepsilon_{\mathrm{D}}(\omega_i,\gamma_i;k,\omega)}\right]=\frac{\omega_i^2\gamma_i\omega}{\left\{\left[\omega_i(k)\right]^2-\omega^2\right\}^2+(\gamma_i\omega)^2}, \quad (7)$$

for finite k; $\omega_i(k)$ is a dispersion term for the plasmon frequency ω_i which was chosen to be $\omega_i(k)=\omega_i+\hbar k^2/2m$ in order to approach the Bethe ridge as $k\to\infty$.[6] It is worth mentioning that both the Mermin ELF and the Drude ELF converge in the optical limit, so that the fitting at $k=0$ by both models yields the same result. The coefficients A_i and B_i representing the relative weight of the Mermin and Drude ELFs, respectively, are related by $B_i=A_i\omega_i^2$.

Penn model

Penn proposed a simpler scheme[7] where the sum over a finite number of Drude-type ELFs is replaced by an integration over Lindhard dielectric functions of zero width. This integration yields the following evolution for finite k[8]

$$\mathrm{Im}\left[\frac{-1}{\varepsilon(k,\omega)}\right]_{\mathrm{outer}}=\frac{\omega'(k)}{\omega}\mathrm{Im}\left[\frac{-1}{\varepsilon(k=0,\omega'(k))}\right]_{\mathrm{outer}}, \quad (8)$$

where $\omega'(k)=\omega-\hbar k^2/2m$. If $\omega'<0$, then $\mathrm{Im}\left[-1/\varepsilon(k,\omega)\right]$ is set to zero. In this way, the optical ELF is easily extended to $k\neq 0$. For comparison with the two previous models, we use the same fitting parameters for the optical ELF resulting from the outer-shell electrons.

Both, the extended Drude and the Penn models describe the ELF corresponding only to outer-shell electrons, and the contribution to the ELF coming from the inner-shell electrons is described in terms of GOS functions for these two models in the same way as is done in the MELF-GOS model. Therefore, when comparing the ELF at finite k in the three models, only the differences in the ELF corresponding to outer-shell electrons will emerge.

Energy loss of H projectiles

When a proton penetrates a material it captures and loses target electrons dynamically modifying its charge state. As soon as charge equilibrium is reached, the stopping power S_{p} of the material can be written as a weighted average of the stopping power for protons, $S_{\mathrm{p},1}$, and hydrogen, $S_{\mathrm{p},0}$:

$$S_{\mathrm{p}}=\phi_0 S_{\mathrm{p},0}+\phi_1 S_{\mathrm{p},1}, \quad (9)$$

where ϕ_q is the charge fraction of the charge state q, which is obtained using the CasP code.[29] In the same way, the energy-loss straggling Ω^2 can be expressed as the sum

$$\Omega^2=\phi_0\Omega_0^2+\phi_1\Omega_1^2. \quad (10)$$

The stopping power and energy-loss straggling for each charge state q is obtained through Eqn. (1) with the limits of the integrals corresponding to particles much heavier than electrons.

IMFP of electrons

When the projectile is an electron, the key magnitude of interest is the IMFP, which is required for quantitative surface spectroscopy techniques.[3] The IMFP of electrons is also obtained from Eqn (1), but as the electronic states under the Fermi energy E_{F} are all occupied by the target electrons, the energy transferred by an electron of energy E cannot exceed $E-E_{\mathrm{F}}$. In addition, due to the indistinguishability between the incident electron and a secondary electron, the maximum energy transfer must be lower than $E/2$. Hence

$$\omega_{\max}=\min\left(\frac{E}{2\hbar},\frac{E-E_{\mathrm{F}}}{\hbar}\right). \quad (11)$$

Results

The optical limit of the ELF for Au and Al is depicted in Fig. 1. The solid lines represent our fitted ELF, with the parameters corresponding to the outer-electron excitations (see Eqn. (3)) given in Table 1 . The circles correspond to experimental data of the ELF,[5] and the triangles were obtained from experimental X-ray scattering factors.[30] The broad spectrum observed in Au is due to the presence of a large number of interband transitions that overlap and interact with collective oscillations.[31] It is then necessary to use seven Mermin-type ELFs to fit correctly the experimental ELF corresponding to the outer-shell excitations. On the other side, Al behaves as a free electron gas, and so, the optical ELF displays a single sharp peak at the plasmon energy; consequently, the optical ELF was fitted by a single Mermin function.

A perspective view of the extension of the ELF of Au into the (k,ω)-space (Bethe surface) is displayed in Fig. 2. We observe that the three models analyzed here give rise to different ELFs at finite k. The positions of the ELF peaks present at $k=0$ are shifted in ω for both the extended Drude model and the Penn model, but the ELFs retain the general shape of the optical spectrum. In contrast, the Mermin model produces an ELF at finite k where the peaks are smeared out, changing the shape of the optical ELF. This effect

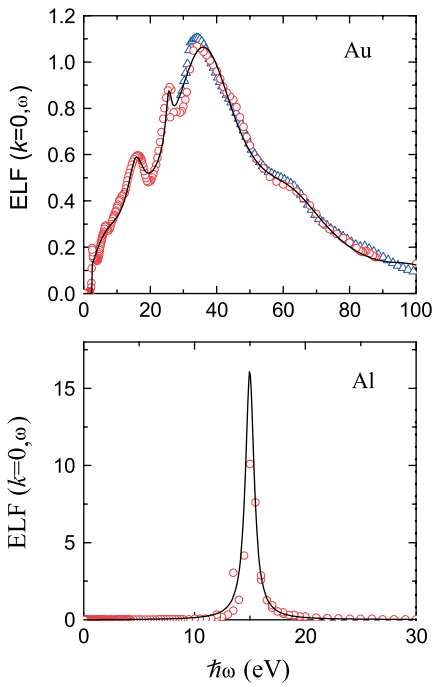

Figure 1. Energy-loss function of Au and Al, in the optical limit ($k=0$), as a function of the excitation energy. The solid lines represent our model, circles are experimental data[5] and triangles are obtained from the X-ray scattering factors.[30] This figure is available in colour online at www.interscience.wiley.com/journal/sia

Table 1. Parameters used to fit the outer-shell electron contributions to the optical ELF of Au and Al. $\mathcal{N}$ is the atomic density of the target.

Target	i	$\hbar\omega_i$ (eV)	$\hbar\gamma_i$(eV)	A_i	$\hbar\omega_{\mathrm{th},i}$ (eV)
Au	1	9.52	14.97	$2.04 \cdot 10^{-1}$	2.5
$\mathcal{N} = 5.90 \cdot 10^{22}$ at/cm^3	2	15.92	6.26	$1.02 \cdot 10^{-1}$	2.5
	3	25.58	2.18	$1.7 \cdot 10^{-2}$	2.5
	4	38.09	26.67	$6.71 \cdot 10^{-1}$	2.5
	5	64.49	30.48	$1.22 \cdot 10^{-1}$	2.5
	6	99.32	19.05	$9.01 \cdot 10^{-3}$	2.5
	7	402.71	612.23	$2.08 \cdot 10^{-2}$	2.5
Al	1	14.99	0.95	1.1178	0.0
$\mathcal{N} = 6.03 \cdot 10^{22}$ at/cm^3					

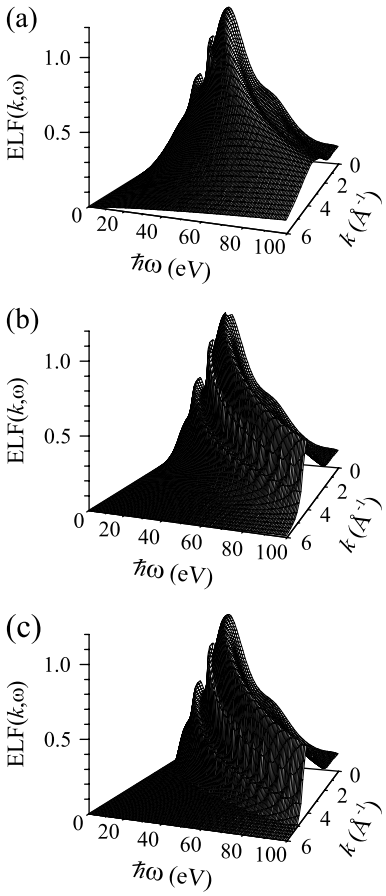

Figure 2. Energy-loss function of Au in the (k, ω)-space, as calculated by (a) the MELF-GOS model, (b) the extended Drude model and (c) the Penn model.

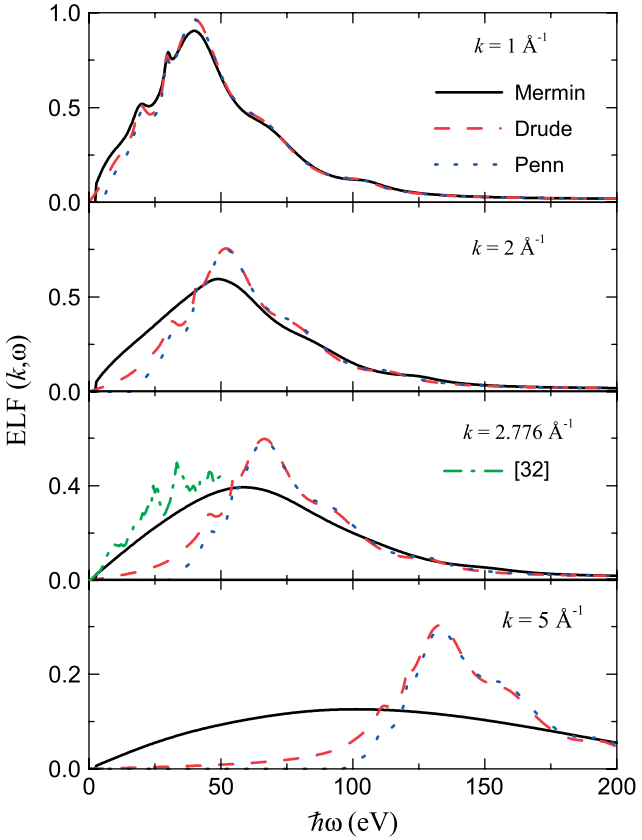

Figure 3. Energy-loss function of Au for different values of k, as indicated in the figure. Solid lines correspond to the MELF-GOS model, dashed lines to the extended Drude model and dotted lines to the Penn model. Dash-dotted lines appearing for $k = 2.776$ Å^{-1} correspond to an *ab initio* calculation made by Gurtubay *et al.*[32] This figure is available in colour online at www.interscience.wiley.com/journal/sia

can be better appreciated in Fig. 3, where we have depicted the evolution of the ELF of Au with different k provided by the three models. At $k = 1$ Å^{-1}, the ELF calculated with the three models almost coincides. However, the Mermin model, represented by the solid lines, predicts a wider spectrum at larger values of k, in which the peaks of the optical ELF have been smeared out. In the Drude and Penn models, the shape of the optical ELF is retained up to $k = 5$ Å^{-1}. The dispersion with k represented by the maximum of the ELF curve is less pronounced in the Mermin model. Although there is no experimental data of the Au ELF at finite k to decide which model produces the more realistic evolution, we have compared the three models at $k = 2.776$ Å^{-1} with the *ab initio* calculation of the dynamical response of Au made by Gurtubay *et al.*,[32] represented by the dash-dotted lines. The agreement of this calculations with the results produced by the MELF-GOS model is rather good, in contrast to the results obtained from the extended Drude and Penn models. In Fig. 4, we have represented the evolution of the ELF of Al with k. The same conclusions drawn for Au apply also for Al. In this case, we have included in the figure the experimental results of energy-loss spectroscopy obtained by Batson and Silcox,[14] represented by dash-dotted lines. We can observe that the ELF from the MELF-GOS model is much more realistic than the other two models which continues to exhibit a sharp peak at finite k. In other materials where experimental data for the ELF at finite k are available (like graphite and liquid water) the MELF-GOS model has been shown to produce a more realistic description of the ELF[19,22] than the extended Drude model. The broadening of the Bethe surface observed experimentally is consistent with the theoretical expectation that single-particle excitations should gradually prevail over collective excitation with increasing k.

This difference in the evolution of the ELF at finite k could have an influence on the calculation of the basic magnitudes of the energy loss of projectiles. In order to elucidate this question we have obtained the stopping power and the energy-loss straggling of Au and Al for protons as a function of the incident

SURFACE and INTERFACE ANALYSIS

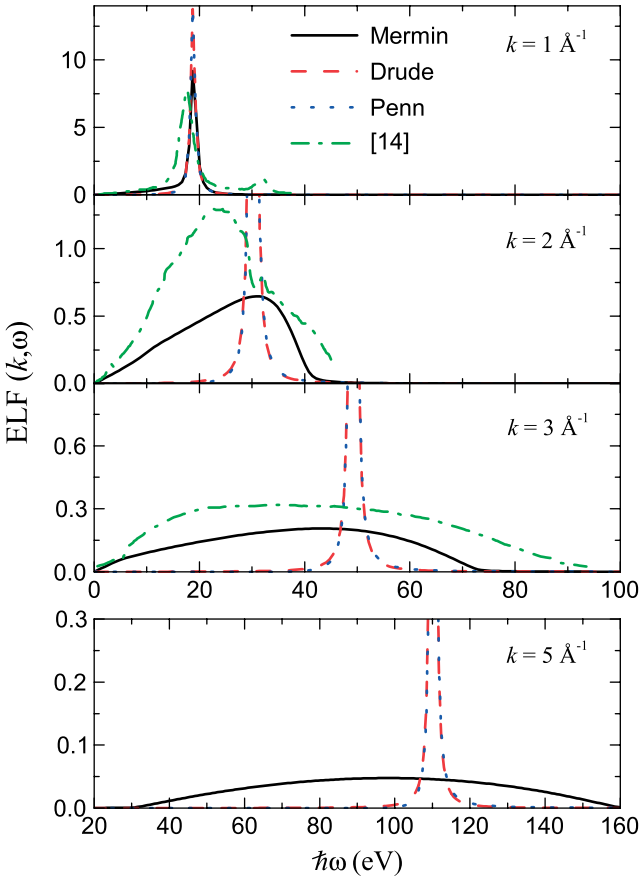

Figure 4. Energy-loss function of Al for different values of k, as indicated in the figure. Solid lines correspond to the MELF-GOS model, dashed lines to the extended Drude model and dotted lines to the Penn model. Dash-dotted lines are experimental data from Batson and Silcox.[14] This figure is available in colour online at www.interscience.wiley.com/journal/sia

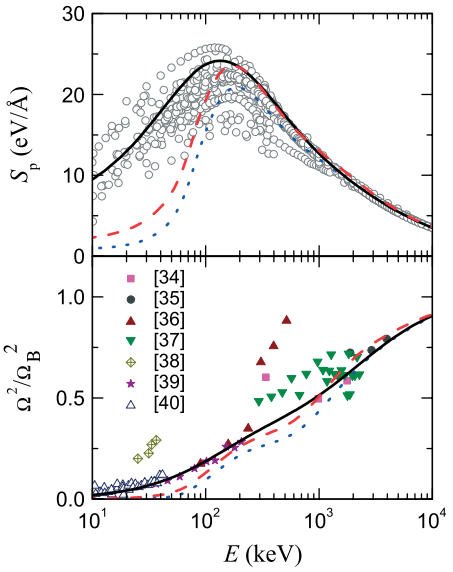

Figure 5. Stopping power and normalized energy-loss straggling of Au for protons as a function of their incident energy. The calculations were done using the MELF-GOS model (full lines), the extended Drude model (dashed lines) and the Penn model (dotted lines). The symbols in the stopping power graph are the re-compilation of experimental data made by Paul,[33] while the symbols in the energy-loss straggling graph are experimental data from Refs.[34–40] This figure is available in colour online at www.interscience.wiley.com/journal/sia

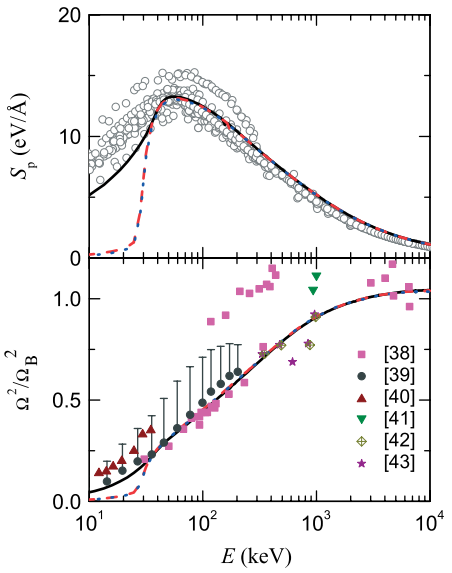

Figure 6. Stopping power and normalized energy-loss straggling of Al for protons as a function of their incident energy. The calculations were done using the MELF-GOS model (full lines), the extended Drude model (dashed lines) and the Penn model (dotted lines). The symbols in the stopping power graph are the re-compilation of experimental data made by Paul,[33] while the symbols in the energy-loss straggling graph are experimental data from Refs.[38–43] This figure is available in colour online at www.interscience.wiley.com/journal/sia

energy, which are shown in Figs. 5 and 6, respectively. The solid lines represent the calculations using the MELF-GOS model, the dashed lines correspond to the extended Drude model and the dotted lines are the results using the Penn model, while the symbols are the available experimental data.[33–43] The energy-loss straggling is represented normalized to the Bohr straggling, given by $\Omega_B^2 = 4\pi e^4 \mathcal{N} Z_1^2 Z_2$. We observe in Fig. 5 that the stopping power of Au agrees in the three models at proton energies above 1000 keV. However, at intermediate and lower energies, there are important differences in the predictions of the three models. At energies below 200 keV, the extended Drude and Penn models have a pronounced descent in the stopping power. As it will be shown in the following, this descent is caused by the incorrect description of the single-electron excitations at small k. The comparison with experiments suggests that the MELF-GOS model provides the more realistic ELF description. Although the energy-loss straggling for Au is less influenced than the stopping power by the model used to describe the ELF, there are important differences which are more noticeable at lower projectile energies, and again, the MELF-GOS method provides the better agreement with the experimental results. Figure 6 shows the case of protons incident on an Al targets. We observe that the three models agree at proton energies above $\sim$ 30 keV. At lower energies the extended Drude model and the Penn model exhibit a pronounced descent in the stopping power and in the energy-loss straggling, which can be understood by the following reasoning. The optical ELF of Al is mainly constituted by a single peak corresponding to the collective excitations of the valence-band electrons. Therefore, the extended Drude and the Penn models, which obtain the ELF evolution using a single Drude function, do not describe correctly the individual

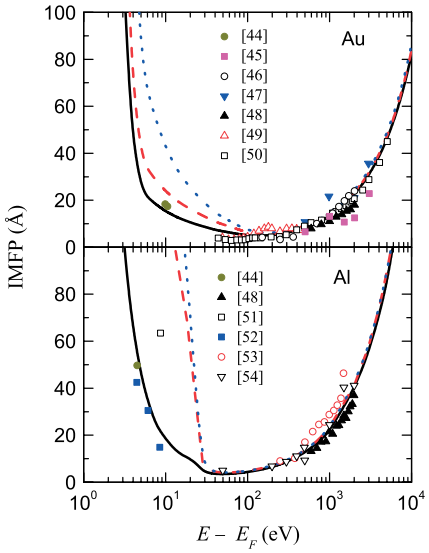

Figure 7. Inelastic mean free path of electrons in Au and Al as a function of their energy. The calculations were done using the MELF-GOS model (full lines), the extended Drude model (dashed lines) and the Penn model (dotted lines). The symbols are the experimental data from the indicated Refs. [44-54] This figure is available in colour online at www.interscience.wiley.com/journal/sia

excitations at small k. If the projectile velocity v is lower than the Fermi velocity of the target v_F, the proton does not produce electronic excitations in the extended Drude or the Penn model. In contrast, the ELF described by the MELF-GOS model behaves at small k like a Lindhard ELF giving the correct description of the individual excitations. At large projectile velocities, large-k individual excitations are well described by a Drude function, and hence, the three models agree in the predictions. The incorrect description of the small-k individual excitations by the extended Drude and Penn models is also present in the case of Au, but as the optical ELF of Au has multiple peaks, the decrease is not so pronounced.

We have also studied the influence of the ELF description on the IMFP of electrons. In Fig.7 we show the calculations of the IMFP as a function of electron energy E above the Fermi level of Au and Al targets. The solid lines are the calculations using the MELF-GOS model, the dashed lines are the results obtained with the extended Drude model, while the results obtained with the Penn model are represented by dotted lines. The symbols are the available experimental data.[44–54] The first attempts to measure IMFPs had large scatter due to lack of film uniformity.[55] Furthermore, due to effects of elastic scattering, these experiments did not measure the IMFP but what is now called the effective attenuation length.[56] Note that we have included in the figure experimental data that were measured after 1990. The only exceptions were Refs. [44,51,52] because these papers reported results of IMFP for electrons with energies under 50 eV. We observe that the three models predict similar values of IMFPs at energies above 100 eV. However, at lower energies, the calculated IMFP of electrons in Au using the MELF-GOS model can be 45% (90%) lower than that obtained with the extended Drude (Penn) model at electron energies of $\sim$ 50 eV. The comparison with experimental data seems to confirm that the MELF-GOS model provides the better agreement, especially in Al. The three models also agree with the IMFP values recommended in Ref. [55], which result from fits to calculated IMFPs from several groups for electron energies ranging from 50 to 10^4 eV.

De la Cruz and Yubero[28] have also found similar differences in IMFP calculations of electrons in several materials, depending on the model used for the ELF description. On the other hand, Akkerman *et al.*[57,58] stated that the calculation of the stopping power and the IMFP is unaffected by the model chosen for the momentum transfer extension ($k \neq 0$), but we have found here that this statement is valid only for large projectile energies.

Conclusions

We use the MELF-GOS model, the extended Drude model, and the Penn model to obtain the ELF of Au and Al from optical data for finite k. Among the three models, we observe that the MELF-GOS model leads to an ELF at finite k where the structure of the optical ELF is distorted, unlike the two other models where the shape of the optical ELF is retained. The different descriptions of the ELF lead to differences in the calculations of the stopping power and energy-loss straggling of Au and Al for protons, especially for low and intermediate projectile energies. At these energies, the MELF-GOS model provides higher values of the stopping power and of the energy-loss straggling for protons, in better agreement with experiments, than both the extended Drude model and the Penn model. In a free-electron gas material, such as Al, the three models agree in the calculation of the stopping power and of the energy-loss straggling for protons at projectile velocities above the Fermi velocity of the material.

The calculation of the IMFP of electrons also depends on the model chosen to calculate the ELF. At projectile energies larger than 100 eV, the three models yield similar results, but at lower electron energies the predictions of the three models can differ significantly. Comparison with experiments suggests that the MELF-GOS model provides the more reliable description of the ELF at finite k.

It is important to emphasize that the same theory has been applied to treat the energy loss of electrons and heavier particles over a broad range of projectile energies. In the case of electrons, we analyze energies of hundreds of eV that can be useful for surface-spectroscopic techniques like AES or XPS.[59] We also study the range of energies under 100 eV, normally not reported in the bibliography, that can be useful for UPS or studies of the valence band and of the Fermi surface.[59,60] For heavier projectiles (protons) we study the energy loss in the range of keVs or MeVs used in several analytical techniques like RBS or PIXE, or several applications, such as implantation of ions or tumor treatment.[1,2]

Acknowledgements

This work was supported by the Spanish Ministerio de Educación y Ciencia (Projects FIS2006-13309-C02-01 and FIS2006-13309-C02-02) and Universitat d'Alacant by Project GRE07-1P. CDD thanks the Spanish Ministerio de Educación y Ciencia and Generalitat Valenciana for support under the Ramón y Cajal Program.

References

[1] E. B. Podgoršak, *Radiation Physics for Medical Physicist*, Springer, Berlin, **2006**.
[2] J. R. Tesmer, M. Nastasi, J. C. Barbour, C. J. Maggiore, J. W. Mayer (Eds.), *Handbook of Modern Ion Beam Materials Analysis*, Material Research Society, Pittsburgh, **1995**.

[3] W. S. M. Werner, *Appl. Surf. Sci.* **2004**, *235*, 2.
[4] J. Lindhard, *K. Dan, Vidensk. Selsk. Mat.-Fys. Medd.* **1954**, *28*(8), 1.
[5] E. D. Palik, G. Ghosh (Eds.), *The Electronic Handbook of Optical Constants of Solids*, Academic Press, San Diego, **1999**.
[6] R. H. Ritchie, A. Howie, *Philos. Mag.* **1977**, *36*, 463.
[7] D. R. Penn, *Phys. Rev. B* **1987**, *35*, 482.
[8] Z. J. Ding, R. Shimizu, *Scanning* **1996**, *18*, 92.
[9] I. Abril, R. Garcia-Molina, C. D. Denton, F. J. Pérez-Pérez, N. R. Arista, *Phys. Rev. A* **1998**, *58*, 357.
[10] A. P. Sorini, J. J. Kas, J. J. Rehr, M. P. Prange, Z. H. Levine, *Phys. Rev. B* **2006**, *74*, 165111.
[11] S. Heredia-Avalos, R. Garcia-Molina, J. M. Fernández-Varea, I. Abril, *Phys. Rev. A* **2005**, *72*, 052902.
[12] S. Heredia-Avalos, J. C. Moreno-Marín, I. Abril, R. Garcia-Molina, *Nucl. Instrum. Methods B* **2005**, *230*, 118.
[13] J. P. Walter, M. L. Cohen, *Phys. Rev. B* **1972**, *5*, 3101.
[14] P. E. Batson, J. Silcox, *Phys. Rev. B* **1983**, *27*, 5224.
[15] U. Büchner, *Phys. Status Solidi B* **1977**, *81*, 227.
[16] N. Watanabe, H. Hayashi, Y. Udagawa, *Bull. Chem. Soc. Jpn.* **1997**, *70*, 719.
[17] H. Hayashi, N. Watanabe, Y. Udagawa, C.-C. Kao, *Proc. Natl. Acad. Sci.* **2000**, *97*, 6264.
[18] N. D. Mermin, *Phys. Rev. B* **1970**, *1*, 2362.
[19] D. J. Planes, R. Garcia-Molina, I. Abril, N. R. Arista, *J. Electron Spectrosc. Relat. Phenom.* **1996**, *82*, 23.
[20] U. Fano, *Annu. Rev. Nucl. Sci.* **1963**, *13*, 1.
[21] M. Inokuti, J. L. Dehmer, T. Baer, J. D. Hanson, *Phys. Rev. A* **1981**, *23*, 95.
[22] D. Emfietzoglou, I. Abril, R. Garcia-Molina, I. D. Petsalakis, H. Nikjoo, I. Kyriakou, A. Pathak, *Nucl. Instrum. Methods B* **2008**, *266*, 1154.
[23] R. Garcia-Molina, I. Abril, C. D. Denton, S. Heredia-Avalos, *Nucl. Instrum. Methods B* **2006**, *249*, 6.
[24] I. Abril, J. C. Moreno-Marín, J. M. Fernández-Varea, C. D. Denton, S. Heredia-Avalos, R. Garcia-Molina, *Nucl. Instrum. Methods B* **2007**, *256*, 172.
[25] J. C. Moreno-Marín, I. Abril, S. Heredia-Avalos, R. Garcia-Molina, *Nucl. Instrum. Methods B* **2006**, *249*, 29.
[26] S. Heredia-Avalos, I. Abril, C. D. Denton, J. C. Moreno-Marín, R. Garcia-Molina, *J. Phys.: Condens. Matter* **2007**, *19*, 466205.
[27] C. C. Montanari, J. E. Miraglia, S. Heredia-Avalos, R. Garcia-Molina,I. Abril, *Phys. Rev. A* **2007**, *75*, 022903.
[28] W. De la Cruz, F. Yubero, *Surf. Interface Anal.* **2007**, *39*, 460.
[29] P. L. Grande, G. Schiwietz, CasP, Convolution Approximation for Swift Particles, version 3.1, **2004**, code available at http://www.hmi.de/people/schiwietz/casp.html.
[30] B. L. Henke, E. M. Gullikson, J. C. Davis, *At. Data Nucl. Data Tables* **1993**, *54*(2), http://xray.uu.se/hypertext/henke.html.
[31] H. A. E. Hagelin-Weaver, J. F. Weaver, G. B. Hoflund, G. N. Salaita, *J. Alloys Compd.* **2005**, *393*, 93.
[32] I. G. Gurtubay, J. M. Pitarke, M. Campillo, A. Rubio, *Comput. Mater. Sci.* **2001**, *22*, 123.
[33] H. Paul, Experimental Stopping Power Compilation, available at http://www.exphys.uni-linz.ac.at/Stopping/ [Accessed January 2008].
[34] W. Möller, U. Nochen, *Nucl. Instrum. Methods* **1978**, *149*, 177.
[35] F. Besenbacher, J. U. Andersen, E. Bonderup, *Nucl. Instrum. Methods* **1980**, *168*, 1.
[36] E. Friedland, C. P. Kotze, *Nucl. Instrum. Methods* **1981**, *191*, 490.
[37] H. W. Alberts, J. B. Malherbe, *Radiat. Eff.* **1983**, *69*, 231.
[38] Q. Yang, D. J. O'Connor, Z. Wang, *Nucl. Instrum. Methods B* **1991**, *61*, 149.
[39] J. C. Eckardt, G. H. Lantschner, *Nucl. Instrum. Methods B* **2001**, *175–177*, 93.
[40] H. H. Andersen, A. Csete, T. Ichioka, H. Knudsen, S. P. Möller, U. I.Uggerhöj, *Nucl. Instrum. Methods B* **2002**, *194*, 217.
[41] Y. Kido, T. Hioki, *Phys. Rev. B* **1983**, *27*, 2667.
[42] Y. Kido, *Phys. Rev. B* **1986**, *34*, 73.
[43] Y. Kido, *Nucl. Instrum. Methods B* **1987**, *24–25*, 347.
[44] H. Kanter, *Phys. Rev. B* **1970**, *1*, 522.
[45] B. Lesiak, A. Jablonski, G. Gergely, *Vacuum* **1990**, *40*, 67.
[46] W. Dolinski, S. Mroz, J. Palczynski, B. Gruzza, P. Bondot, A. Porte, *Acta Phys. Pol.* **1992**, *A81*, 193.
[47] G. Gergely, M. Menyhard, K. Pentek, A. Sulyok, A. Jablonski, B. Lesiak, C. Daroczi, *Vacuum* **1995**, *46*, 591.
[48] A. Koch, Ph.D. Thesis, Physics Department, Eberhard-Karls-Universität, Tübingen, **1996**.
[49] A. Jablonski, P. Jiricek, *Surf. Sci.* **1998**, *412–413*, 42.
[50] S. Tanuma, T. Shiratori, T. Kimura, K. Goto, S. Ichimura, C. J. Powell, *Surf. Interface Anal.* **2005**, *37*, 833.
[51] T. Huen, F. Wooten, *Solid State Commun.* **1971**, *9*, 871.
[52] T. A. Callcott, E. T. Arakawa, *Phys. Rev. B* **1975**, *11*, 2750.
[53] H. Beilschmidt, I. S. Tilinin, W. S. M. Werner, *Surf. Interface Anal.* **1994**, *22*, 120.
[54] B. Lesiak, A. Jablonski, L. Zommer, A. Kosinski, G. Gergely, A. Konkol, A. Sulyok, Cs. S. Daroczi, P. Nagy, in *Proceedings of the 6th European Conference on Applications of Surface and Interface Analysis: ECASIA95*, Montreaux 1995 (Eds: H. J. Mathieu, B. Reihl, D. Briggs), Wiley, Chichester, **1996**.
[55] C. J. Powell, A. Jablonski, *J. Phys. Chem. Ref. Data* **1999**, *28*, 19.
[56] A. Jablonski, C. J. Powell, *Surf. Sci. Rep.* **2002**, *47*, 33.
[57] A. Akkerman, E. Akkerman, *J. Appl. Phys.* **1999**, *86*, 5809.
[58] A. Akkerman, A. Breskin, R. Chechik, Y. Lifshitz, *Radiat. Phys. Chem.* **2001**, *61*, 333.
[59] D. P. Woodruff, T. A. Delchar, *Modern Techniques of Surface Science*, *Cambridge Solid State Sciences Series*, Cambridge University Press, Cambridge, **1994**.
[60] S. Huffner, *Photoelectron Spectroscopy: Principles and Applications*, *Springer Series in Solid-state Science*, Springer-Verlag, Berlin, **2003**.

